

Third-Order Aperture Mass Statistics of Cosmic Shear

M. Kilbinger and P. Schneider

Institut für Astrophysik und Extraterrestrische Forschung, Universität Bonn, Auf dem Hügel
71, D-53121 Bonn

Abstract. We present predictions for cosmological parameter constraints from combined measurements of second- and third-order aperture mass statistics of cosmic shear. The generalized third-order aperture mass is introduced and its relation to the convergence bispectrum is given. This quantity contains (in principle) all information about the bispectrum. Using ray-tracing simulations, we perform a Fisher matrix analysis for various cosmological parameters and show that the combination of $\langle M_{\text{ap}}^2 \rangle$ and $\langle M_{\text{ap}}^3 \rangle$ improves the parameter estimation significantly.

1. Introduction

The majority of cosmic shear observations, using deep surveys ($z \lesssim 1$) with large sky coverage (up to ~ 100 square degree), is up to now based on second-order statistics. Shear two-point functions have been measured with great success, and cosmological parameters, in particular the (dark+luminous) matter density Ω_m and the power spectrum normalization σ_8 have been significantly constrained (e.g. van Waerbeke et al. 2004; Jarvis et al. 2003; Réfrégier et al. 2002; Hoekstra et al. 2002).

Only recently, third-order statistics of cosmic shear have been detected successfully (Bernardeau 2002; Pen et al. 2003; Jarvis et al. 2004), consistent with predictions from the concordance Λ CDM model.

Although the detection of the small amplitude signal of higher-order statistics is very challenging, it contains valuable information about the dark matter distribution in the Universe:

- The large-scale matter distribution in the Universe is non-Gaussian on scales smaller than $\sim 10 h^{-1}$ Mpc, corresponding to angular scales $\lesssim 50'$ for typical redshifts involved for cosmic shear. This non-Gaussianity arises from non-linear gravitational instabilities and is only measurable using higher-order statistics.
- The dependence on cosmological parameters is different for second- and third-order functions of cosmic shear, therefore (near-)degeneracies between cosmological parameters can be lifted by combined measurements. For example, the most prominent Ω_m - σ_8 -degeneracy can be broken using the reduced skewness of the aperture mass statistics $\langle M_{\text{ap}}^3(\theta) \rangle / \langle M_{\text{ap}}^2(\theta) \rangle^2$ which strongly depends on Ω_m but is only a weak function of σ_8 (see Fig. 1, also Schneider et al. 1998; van Waerbeke et al. 1999).

2. Convergence bispectrum

The bispectrum B_κ of the surface mass density κ is defined as

$$\langle \hat{\kappa}(\vec{\ell}_1) \hat{\kappa}(\vec{\ell}_2) \hat{\kappa}(\vec{\ell}_3) \rangle = (2\pi)^2 \delta_D(\vec{\ell}_1 + \vec{\ell}_2 + \vec{\ell}_3) \left[B_\kappa(\vec{\ell}_1, \vec{\ell}_2) + B_\kappa(\vec{\ell}_2, \vec{\ell}_3) + B_\kappa(\vec{\ell}_3, \vec{\ell}_1) \right]; \quad (2.1)$$

it is defined for closed triangles in Fourier space. For a Gaussian random field, the bispectrum vanishes, and different Fourier modes are uncorrelated. In the general case

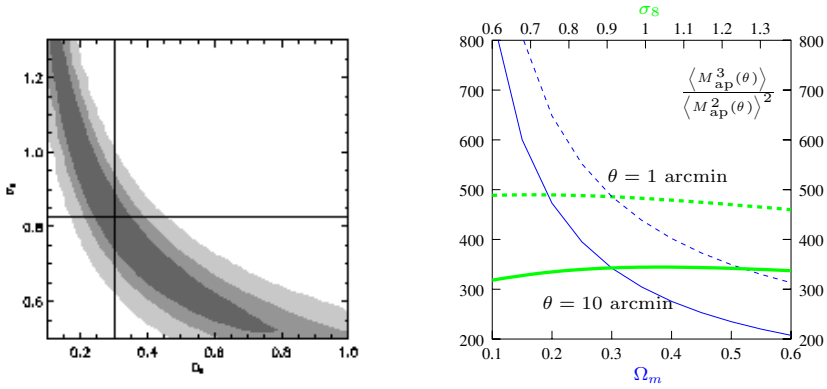


Figure 1. *Left panel:* The measured near-degeneracy between Ω_m and σ_8 (van Waerbeke et al. 2004). *Right panel:* The reduced skewness plotted as a function of Ω_m (thin lines) and σ_8 (thick curves), for two different aperture radii $\theta = 1'$ (dashed) and $\theta = 10'$ (solid). The non-varying parameters are kept fixed to $\Omega_m = 0.3$ and $\sigma_8 = 0.9$ respectively.

however, there are mode couplings – the bispectrum is a measure of the amplitude of these couplings. Because κ is statistically isotropic, the bispectrum can be reparametrized as $B(\vec{l}_1, \vec{l}_2) = b(l_1, l_2, \varphi)$ where $\varphi = \angle(\vec{l}_1, \vec{l}_2)$.

In order to model the bispectrum, we use the ansatz from Scoccimarro & Couchman (2001), called *Hyper-extended perturbation theory* (HEPT). This approach is based on (second-order) perturbation theory (PT). It is a modification of PT on small-scales, obtained by fitting the highly non-linear regime to N-body simulations. In both PT and HEPT, the above defined function b can be written as

$$b(l_1, l_2, \varphi) = \sum_{m=0}^2 \cos^m(\varphi) \bar{b}_\kappa^{(m)}(l_1, l_2). \tag{2.2}$$

3. Aperture mass statistics

3.1. Definition

The aperture mass is defined as a filtered integral over the convergence κ in a circular aperture. It also can be written as a filtered integral over the shear tangential to the aperture center (Kaiser, N. et al. 1994; Schneider 1996):

$$M_{\text{ap}}(\theta) = \int d^2x U_\theta(x) \kappa(\vec{x}) = \int d^2x Q_\theta(x) \gamma_t(\vec{x}). \tag{3.1}$$

The second equality holds if U_θ is a compensated filter, i.e. $\int dx x U_\theta(x) = 0$. Using this relation, it is possible to determine M_{ap} in a local region on the sky, by measuring the tangential ellipticities of galaxies within the aperture, which are estimators of the shear in the weak lensing regime, $\langle \varepsilon_t \rangle = \gamma_t$.

In the following, we will use the filter functions introduced by Crittenden et al. (2002):

$$U_\theta(x) = \frac{1}{2\pi\theta^2} \left(1 - \frac{x^2}{2\theta^2} \right) e^{-\frac{x^2}{2\theta^2}}; \quad Q_\theta(x) = \frac{x^2}{4\pi\theta^4} e^{-\frac{x^2}{2\theta^2}}. \tag{3.2}$$

3.2. Second moment

The second moment or *variance* is of main interest for cosmic shear observations, because it is a direct measure of the power spectrum P_κ of the projected large-scale matter

fluctuations:

$$\langle M_{\text{ap}}^2(\theta) \rangle \equiv \langle M_{\text{ap}}(\theta) M_{\text{ap}}(\theta) \rangle = \frac{1}{2\pi} \int d\ell \ell W(\theta\ell) P_{\kappa}(\ell), \quad (3.3)$$

where the filter function $W(\eta) = \eta^4 \exp(-\eta^2)/4$ is a peaked, localized function, which makes $\langle M_{\text{ap}}^2 \rangle$ a local measure of the power spectrum. By measuring this quantity for different aperture radii θ , the power spectrum can be probed locally and scanned over a large range of wave numbers.

3.3. Third moment

The third moment or *skewness* of the aperture mass $\langle M_{\text{ap}}^3(\theta) \rangle \equiv \langle M_{\text{ap}}(\theta) M_{\text{ap}}(\theta) M_{\text{ap}}(\theta) \rangle$ can be written as a function of the bispectrum of the convergence κ . It is mainly sensitive to wave vectors which form equilateral triangles in Fourier space. It therefore probes basically the diagonal of the bispectrum; we denote this quantity as $\langle M_{\text{ap,d}}^3(\theta) \rangle$.

It is thus very useful to generalize this expression, and define a quantity which is the correlator of M_{ap} using three different filter radii:

$$\langle M_{\text{ap}}^3(\theta_1, \theta_2, \theta_3) \rangle \equiv \langle M_{\text{ap}}(\theta_1) M_{\text{ap}}(\theta_2) M_{\text{ap}}(\theta_3) \rangle \quad (3.4)$$

This quantity probes (in principle) the full ℓ -space of the bispectrum.

With the definition of (2.2), we write $\langle M_{\text{ap}}^3(\theta_1, \theta_2, \theta_3) \rangle$ as a function of the bispectrum:

$$\langle M_{\text{ap}}^3(\theta_1, \theta_2, \theta_3) \rangle = \int d\ell_1 \ell_1 \int d\ell_2 \ell_2 \sum_{m=0}^2 I^{(m)}(\theta_1, \theta_2, \theta_3, \ell_1, \ell_2) \bar{b}_{\kappa}^{(m)}(\ell_1, \ell_2). \quad (3.5)$$

The filter functions $I^{(m)}$, as shown in Fig. 2, are relatively sharply peaked, as in the case of $\langle M_{\text{ap}}^2 \rangle$. Thus, $\langle M_{\text{ap}}^3 \rangle$ is a local measure of the bispectrum. Apparently, $\langle M_{\text{ap,d}}^3 \rangle$ mainly probes the diagonal of the $\bar{b}_{\kappa}^{(m)}$, whereas the generalized third-order aperture mass using different filter radii is sensitive to a larger region in ℓ -space and contains more information about the bispectrum and thus cosmology.

4. Ray-tracing simulations

In order to predict the measurement accuracy of cosmological parameters using second- and third-order aperture statistics of cosmic shear, we use 36 Λ CDM ray-tracing simulations, see Ménard et al. (2003) for details. Each field is a 1024×1024 κ -grid and represents a 12 square degree section of the sky. The source galaxies are situated at a common redshift of $z_0 = 0.977$.

The results for the aperture mass statistics from the ray-tracings match very well the theoretical predictions for filter radii $\theta \gtrsim 1'$, as shown in Fig. 3.

We split up every field in four subfields, and calculate the covariances of $\langle M_{\text{ap}}^2 \rangle$ and $\langle M_{\text{ap}}^3 \rangle$ by averaging over the 144 subfields, neglecting the small correlation between adjacent subfields. Thus, our simulated survey corresponds to a single field with an area of three square degree. To each κ pixel, we add an intrinsic ellipticity as a Gaussian random variable with dispersion $\sigma_{\varepsilon} = 0.3$. Thus, the covariance contains errors both from cosmic variance as well as from intrinsic ellipticities. We verify that our calculation of the covariance from galaxies at grid points instead of (quasi-)random positions introduces no artefacts, and also that no smoothing of the κ field is necessary. We compare the covariance of $\langle M_{\text{ap}}^2 \rangle$ for Gaussianized κ fields with the method from Kilbinger & Schneider (2004) and find excellent agreement between the two approaches.

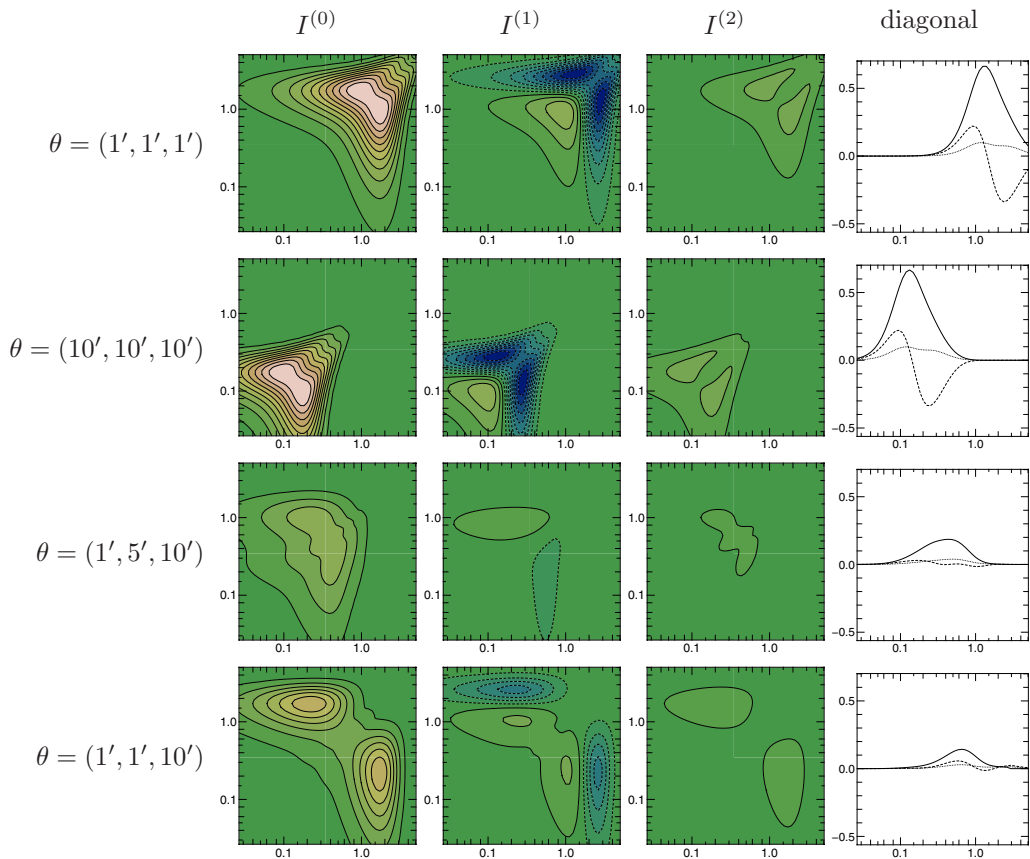


Figure 2. Contours of the integrand $I^{(m)}$ for $m = 0, 1, 2$ from left to right are plotted for different values of θ_i as a function of ℓ_1 and ℓ_2 in units of $h \text{ Mpc}^{-1}$. The right-most panels show the profile of the diagonal of $I^{(m)}$, where the solid, dashed and dotted lines correspond to $m = 0, 1$ and 2 respectively.

5. Constraints on cosmological parameters

In order to quantify the accuracy of the determination of cosmological parameters using second- and third-order aperture mass statistics of cosmic shear, we calculate the Fisher matrix F_{ij} (Tegmark 1997) to get degeneracy directions and amplitudes for different combinations of cosmological parameters. The most important quantity obtained from the Fisher matrix is the minimum variance bound (MBV), the lower bound of the $1\text{-}\sigma$ -uncertainty for any unbiased estimator.

We use four different filter radii $\theta = 1.4, 3.9, 10.8$ and 18 arc minutes and obtain a total of 24 independent data points (4 for $\langle M_{\text{ap}}^2 \rangle$ and 20 for $\langle M_{\text{ap}}^3 \rangle$).

As an illustrative example, we plot the MBV as error ellipses in Fig. 4 for combinations of two parameters. All hidden parameters are kept fixed. Note that a flat Universe is assumed (except in the case where both Ω_m and Ω_Λ enter the Fisher matrix.) Clearly, a substantial improvement is obtained by combining second- and third-order aperture statistics. Also, as expected, the generalized $\langle M_{\text{ap}}^3 \rangle$ gives better constraints than the “diagonal” version of the skewness $\langle M_{\text{ap,d}}^3 \rangle$.

If we include more parameter in our analysis, it is necessary to introduce weak priors, in order to regularize the likelihood function and to keep the MBVs reasonably small. For

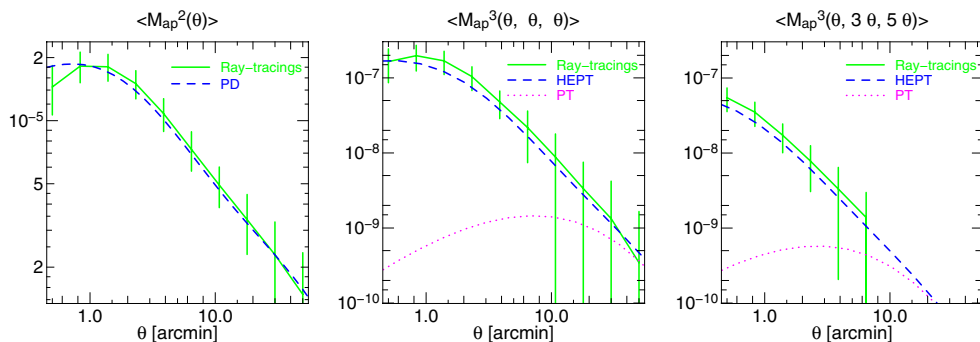


Figure 3. $\langle M_{\text{ap}}^2 \rangle$ and $\langle M_{\text{ap}}^3 \rangle$ from the ray-tracing simulations as compared to theoretical predictions. The error bars are the rms from the 36 fields. PD=Peacock & Dodds (1996).

each parameter, we assume an additional Gaussian prior of unit variance. The absolute values of the MVBs increase with the width of the prior, however the relative MVBs between the different statistics and their combination is only weakly depending on the priors.

In Table 1, the main result of this work is presented. The MVBs for combinations of three and four cosmological parameters are shown for $\langle M_{\text{ap}}^2 \rangle$, the generalized $\langle M_{\text{ap}}^3 \rangle$ and the combination of both measures. The hidden parameters are again fixed; if not both Ω_m and Ω_Λ are varying, a flat Universe is assumed. In all cases, a considerable decrease of the MVBs is obtained combining second- with third-order M_{ap} -statistics.

Constraints on the cosmological constant are very poor; in order to make improvements here, one has to include redshift information and do shear tomography, see e.g. Hu (1999) and Takada & Jain (2004). The uncertainty in the source redshift highly

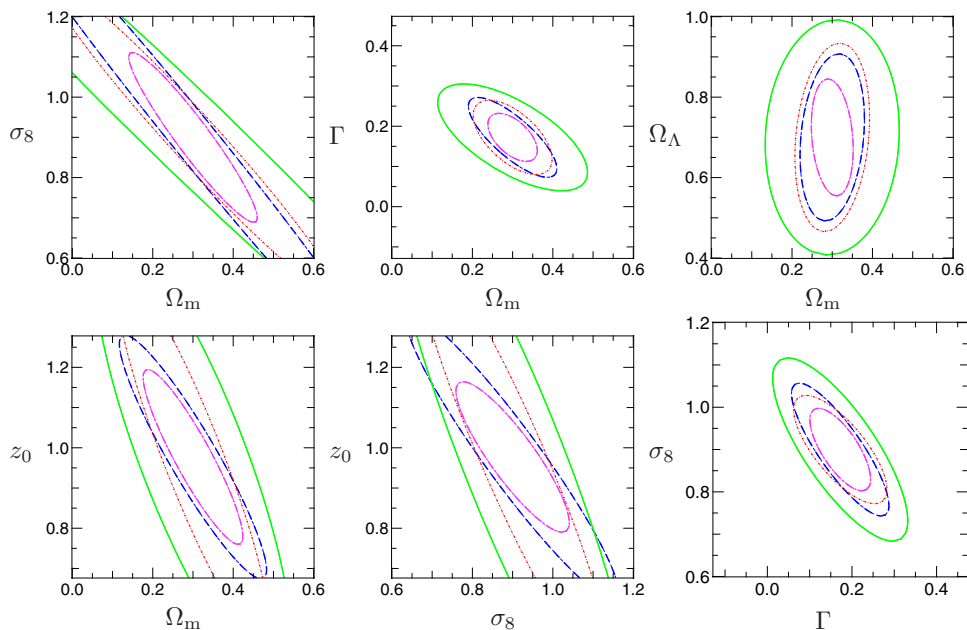


Figure 4. $1\text{-}\sigma$ error ellipses for some combinations of two cosmological parameters. Blue dashed line: $\langle M_{\text{ap}}^2 \rangle$, red dotted line: $\langle M_{\text{ap}}^3 \rangle$, green solid line: $\langle M_{\text{ap}}^3, d \rangle$, violet dash-dotted line: combination of $\langle M_{\text{ap}}^2 \rangle$ and $\langle M_{\text{ap}}^3 \rangle$

increases the errors of all parameters; this fact will most likely also hold for a continuous source redshift distribution instead of a single z -plane. Detailed knowledge about this distribution is therefore of great importance, and it can be obtained by measuring photometric redshifts or by using the z -distribution of other (spectroscopic) galaxy surveys with similar observation parameters.

From Fig. 4, one sees that the directions of degeneracy between parameters are similar for $\langle M_{\text{ap}}^2 \rangle$ and $\langle M_{\text{ap}}^3 \rangle$. However, there are differences, which help to at least partially lift the degeneracies by combined measurements. The figures in Table 1 reveal that in some cases rather large MVBs for $\langle M_{\text{ap}}^2 \rangle$ and $\langle M_{\text{ap}}^3 \rangle$ get much smaller for the combined statistics, which is due to the difference in the directions of degeneracy in parameter space.

Table 1. MVBs for various combinations of three and four cosmological parameters. The hidden parameters are kept fixed. ‘2’, ‘3’ and ‘2+3’ stand for $\langle M_{\text{ap}}^2 \rangle$, $\langle M_{\text{ap}}^3 \rangle$ and the combination of both statistics respectively.

	Ω_{m}	σ_8	Γ	Ω_{Λ}		Ω_{m}	σ_8	Γ	z_0
2	0.44	0.63	0.13		2	0.39	0.54		0.33
3	0.47	0.61	0.16		3	0.31	0.39		0.46
2+3	0.19	0.29	0.09		2+3	0.18	0.21		0.21
2	0.43	0.71	0.44	0.87	2	0.57	0.67	0.28	0.71
3	0.49	0.64	0.35	0.69	3	0.57	0.64	0.21	0.62
2+3	0.23	0.31	0.17	0.60	2+3	0.49	0.50	0.21	0.52

Acknowledgements

We thank Takashi Hamana for kindly providing his ray-tracing simulations.

References

- Bernardeau, F., Mellier, Y. & van Waerbeke, L., 2002, *A&A*, 389, L28
 Crittenden, R. G., Natarajan, P., Pen, U.-L. et al., 2002, *ApJ*, 568, 20
 Hoekstra, H., Yee, H. K. C. & Gladders, M. D., 2002, *ApJ*, 577, 595
 Hu, W., 1999, *ApJ*, 522, L21
 Jarvis, M., Bernstein, G., Fischer, P. et al., 2003, *AJ*, 125, 1014
 Jarvis, M., Bernstein, G. & Jain, B., 2004, *MNRAS*, 352, 338
 Kaiser, N., Squires, G., Fahlman, G. et al., 1994, in *Proc. of the XIVth Moriond Astrophysics Meeting, Clusters of galaxies, Méribel, France*, p. 269
 Kilbinger, M. and Schneider, P., 2004, *A&A*, 413, 465
 Ménard, B., Hamana, T., Bartelmann, M. et al., 2003, *A&A*, 403, 817
 Peacock, J. A. & Dodds, S. J., 1996, *MNRAS*, 280, L19
 Pen, U., Zhang, T., van Waerbeke, L. et al., 2003, *ApJ*, 592, 664
 Réfrégier, A., Rhodes, J. & Groth, E. J., 2002, *ApJ*, 572, L131
 Schneider, P., 1996, *MNRAS*, 283, 837
 Schneider, P., van Waerbeke, L., Jain, B. et al., 1998, *MNRAS*, 296, 873
 Scoccimarro, R. & Couchman, H. M. P., 2001, *MNRAS*, 325, 1312
 Takada, M. & Jain, B., 2004, *MNRAS*, 348, 897
 Tegmark, M., Taylor, A. & Heavens, A., 1997, *ApJ*, 480, 22
 van Waerbeke, L., Bernardeau, F. & Mellier, Y., 1999, *A&A*, 342, 15
 van Waerbeke, L., Mellier, Y. & Hoekstra, H., 2004, preprint (astro-ph/0406468)